Global Flow Measurement Workshop
22-24 October 2024

Technical Paper

Correction for Orifice Plates installed in Reverse Orientation, CFD or Flow Testing?

Dr. Nadezhda Pashnina CEng, Emerson
Paul Daniel, i-Vigilant Technologies Limited
Marc Laing, Dr. Sandy Black, TÜV SÜD
Dr. Aleksandr Terekhin, Denis Ismagilov, South Ural State University

ABSTRACT

This paper examines the impact on the flow measurement in caused by the sequential installation of two orifice plates, one after the other over time, in reverse orientation within an 18-inch gas metering stream over a period of nearly two years. The orifice plates, each with a beta ratio of approximately 0.72, were part of a gas metering system within the UK National Transmission System (NTS) used to determine the Offtake to a Local Distribution Zone (LDZ), with a typical flow rate of approximately 5 million Sm^3/d.

Upon discovering the incorrect installation, it became necessary to quantify the measurement error as it was suspected to be significant. Due to the anticipated magnitude of the measurement error, two Independent Technical Experts (ITEs) were identified and appointed to compile individual Significant Measurement Error Reports (SMERs) independently. To determine the magnitude of the error accurately, ITE 1 undertook Computational Fluid Dynamics (CFD) simulations, and ITE 2 looked at both CFD and in situ flow testing using a clamp-on ultrasonic flow meter (USM). Upon completion of both SMERs the ITEs reviewed each other's reports to identify any material differences and to propose a single conclusion. By combining the results, the measurement errors were estimated to range from 3 % to 8 %.

This paper will be particularly useful for engineers and professionals involved in flow measurement, especially those working in gas metering systems, as it provides insights into correcting flow measurement errors caused by reverse installation of orifice plates using both CFD and flow testing methodologies.

Keywords: orifice plate; reverse orientation; flow measurement error; CFD; in situ flow testing; clamp-on USM

1 INTRODUCTION

Orifice plates are among the most widely used devices in flow measurement for determining the flow rate in pipelines where a fluid is running full. The presence of a restriction (the orifice) in a pipe creates a static pressure difference between the upstream and downstream sides of the plate, and this pressure drop correlates with the flow rate of the fluid passing through the orifice, as detailed in ISO 5167-2:2003 [3].

The accurate determination of the flow rate using this method depends heavily on the proper installation of the orifice plate in the metering stream. In particular, the plate must be oriented with the sharp edge facing the upstream flow, or forward orientation. The sharp edge allows the flow to separate correctly, ensuring that the calculated discharge coefficient remains accurate. The flow separation occurs downstream of the orifice edge, where the flow cannot follow the sharp contour of the plate and instead separates from the surface.

However, when an orifice plate is installed in reverse orientation, with the bevelled edge facing upstream and the square edge facing downstream, significant measurement errors can occur. The flow behaviour changes, which affects the separation region downstream of the plate. In this reverse orientation, the flow gradually turns along the bevel of the orifice plate,

forming several zones of flow separation along the bevel edge. This results in a pressure drop reduction across the plate, leading to a higher discharge coefficient and, consequently, an underestimation of the actual flow rate if the discharge coefficient for the correct orientation is used in calculations.

In flow measurement systems, orifice plates are regularly removed and inspected to ensure they are not damaged or contaminated. During this process, there is a possibility that, after inspection or replacement, the orifice plate may be installed in the reverse orientation. Such installation errors of an orifice plate can go unnoticed for long periods, leading to significant measurement errors. This issue is particularly critical in high-accuracy applications, such as gas metering for custody transfer and allocation purposes, where even small inaccuracies can result in substantial financial losses.

It is standard practice for reported figures to be recalculated and agreed upon by the relevant parties, in accordance with appropriate standards. However, in this case of a reversed orifice plate, the published literature does not contain sufficient information to enable the measurement error to be calculated from the geometry of the orifice plates alone with any great confidence. Paper [1] indicates that an orifice plate with a beta ratio of approximately 0.6, installed in the reverse orientation in a 10-inch stream, can result in an undermeasurement of up to 22 % ± 3 %.

Paper [4] provides the equation to determine the measurement error caused by the reverse installation of an orifice plate and suggests that the error is (1) a strong function of the orifice beta ratio β, (2) a moderately strong function of the ratio of orifice bore thickness to plate thickness, e/E, (3) a moderately strong function of the ratio of orifice plate thickness to meter tube diameter, E/D, and (4) a very weak function of Reynolds number. According to this equation, the error for the orifice plates of interest is estimated to be approximately 9 %.

To assess the measurement error caused by the reverse installation of these orifice plates, similarly to paper [1], two approaches were selected: CFD, which provides a theoretical approach through modelling, and experimental flow testing using USM.

The objective of this paper is to assess how well the results of the two approaches align, determine whether CFD can independently provide satisfactory results, and offer guidance on correcting flow measurement errors caused by reversed orifice plates.

To achieve this, the following steps have been taken:

- **CFD Simulations**: Both TÜV SÜD (NEL) and Emerson in cooperation with South Ural State University (SUSU) performed CFD simulations to model the flow through the orifice plates in both forward and reverse orientations. The simulations aimed to calculate the change in discharge coefficient due to the reversed orientation and to validate the results using industry standards and published data.
- **Flow Testing**: i-Vigilant Technologies conducted flow tests using a clamp-on ultrasonic flow meter. The flow tests were performed with the orifice plates in both forward and reverse orientations to measure the difference in flow rate and establish the extent of undermeasurement.
- **Comparison and Analysis**: The results from the CFD simulations and flow tests are compared to assess their accuracy and reliability.

2 INSTALLATION DESCRIPTION

The layout of the National Transmission System (NTS) Offtake to Local Distribution Zone (LDZ) is shown on Figure 1. A flow element (orifice plate) is installed in a pipeline carrying natural gas. The upstream straight length is 49 D after a 45-degree bend and a valve, and it includes a flange connection 23 D upstream from the orifice plate, where a flow conditioner may be installed. The upstream straight length is 22.5 D.

Figure 1 – Metering Stream Layout

The details of the orifice fitting, orifice plates, and process conditions are tabulated below. The orifice plate dimensions are explained in Figure 2.

Table 1 – Orifice Plate Parameters

Parameter	**Units**	**Plate No 1**	**Plate No 2**
Bore Diameter 'd' at Calibration and Process Temperature	mm	309.9971 at 19.5 ºC 309.9425 at 8.5 ºC	310.0018 at 20.0 ºC 309.9448 at 8.5 ºC
Temperature Expansion Factor	1/ºC	0.000016	0.000016
Plate Thickness 'E'	mm	9.2370	9.2873
Orifice Bore Thickness 'e'	mm	7.015	7.450
b=E-e	mm	2.222	1.8373
b/d (e/E)	-	0.007 (0.7594)	0.006 (0.8022)
Angle of Bevel 'α'	°	44.50	44.00
Beta Ratio 'β'	-	0.71695	0.71696
Distance between Tappings	mm	60.0370	60.0873

Table 2 – Orifice Fitting and Pipe Parameters

Parameter	**Units**	**Value**
Upstream Diameter 'D' at Calibration and Process Temperature	mm	432.36 at 20.0 ºC Calibration 432.3053 at 8.5 ºC Process
Temperature Expansion Factor	1/ºC	0.000011
Upstream Straight Length	m	10.06158
Downstream Straight Length	m	3.19723
Tappings	-	Flange
Distance of Tappings from Orifice Plate	mm	25.4
Tapping Diameter	mm	6

Table 3 – Process Conditions

Parameter	**Units**	**Value**
Typical Flowing Pressure	barg	56
Typical Flowing Temperature	ºC	8.5
Typical Standard Volume Flow	Sm^3/h	175,000
Typical Mass Flow	kg/h (kg/s)	131,659.50 (36.57)
Typical Velocity	m/s	4.9502
Typical Reynolds Number	-	8.95E+06
Gas Molecular Weight	kg/kmol	17.7472
Compressibility Factor	-	0.85843
Process Density 'ρ_1'	kg/m^3	50.3333
Dynamic Viscosity	cP	0.01204

The axial plane cross-section of the orifice plates No 1 and No 2 at process conditions are shown in Figure 2 along with the explanation of letters obtained from ISO 5167-2 [3].

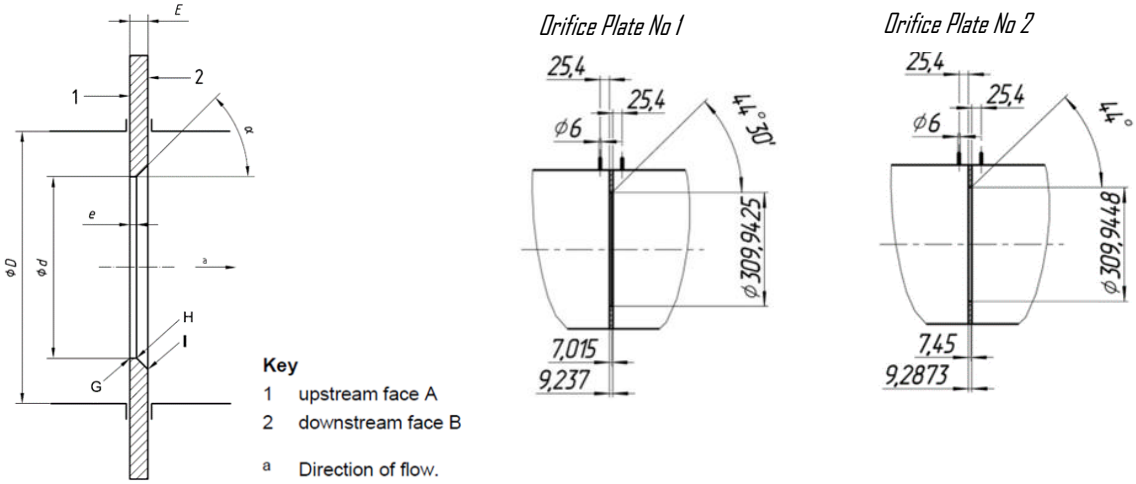

Figure 2 – 2D Geometry of Orifice Plates

3 CFD STUDY OF REVERSED ORIFICE PLATES

To assess the change in discharge coefficient, a series of simulations were conducted using CFD. Simulations were performed for both orifice plates in forward and reverse orientations, allowing for a comparison between the results. A well-established CFD software package was utilised for modelling. The modelling was performed by two independent ITEs: NEL utilised ANSYS Fluent solver 2021 R1, while SUSU employed two solvers ANSYS CFX and ANSYS Fluent 2019 R3 configured independently by the two specialists.

In general, CFD modelling involves four steps: (1) creating the model geometry, (2) creating the mesh (a mesh is the collection of small elements (finite volumes) into which a 3D model geometry is divided, allowing the non-linear partial differential equations governing fluid flow to be solved numerically within each element), (3) defining the physical models by the model setup, and (4) defining the boundary and operating conditions.

The following sections will detail the approaches and results of modelling delivered independently by the two ITEs. The summary of taken approaches is shown in Table 4.

Table 4 – Summary of Approaches to CFD Modelling

	NEL	**Emerson (SUSU)**
CFD Solver Name	ANSYS Fluent	ANSYS CFX, ANSYS Fluent
CFD Solver Version	2021 R1	2019 R3
Plate Geometry	Laser Scanning	Calibration Certificates
Turbulence Model	k-ε	k-ω SST
Mesh Type	unstructured polyhedral	structured hexahedral
Number of Elements	40 million	0.5 million
Element Size around Orifice Plate	0.2 mm	0.1 mm
Model Validation in Forward Orientation	ISO 5167-2 [3]	ISO 5167-2 [3]
Model Validation in Reverse Orientation	GRI Report 01/0074 [2]	NSFMW Paper [1]

In both approaches the discharge coefficient is evaluated using the standard equation (1), where the mass flow rate is defined as a boundary condition at the inlet of the model, the pressure drop is evaluated by the CFD computation results, and other parameters are defined in Table 1 and Table 3 of section 2.

$$\mathbf{C \cdot \varepsilon = \frac{q_m \cdot \sqrt{1 - \beta^4}}{\frac{\pi \cdot d^2}{4} \cdot \sqrt{2 \cdot \Delta p \cdot \rho_1}}} \quad (1)$$

Where:

q_m	is the mass flow rate, kg/s
C	is the discharge coefficient, dimensionless
β	is the diameter ratio under upstream process conditions, dimensionless
d	is the orifice bore diameter at upstream temperature, m
D	is the internal pipe diameter at upstream temperature, m
ε	is the expansibility factor, dimensionless
Δp	is the differential pressure (pressure drop), Pa
ρ_1	is the upstream process density, kg/m^3

3.1 CFD Approach by NEL

The first computational approach was carried out by NEL. The orifice plates used in this study were laser-scanned to obtain precise geometrical data. The plate geometry is important as even small variations in bevel dimensions or edge thickness could significantly affect the flow characteristics. NEL used an **unstructured polyhedral mesh** with refinements around the plate. The mesh independence study was performed. Three Reynolds numbers were selected for the simulations. The **k-ε realisable turbulence model** was applied due to its effectiveness in handling separated flows.

The simulations were performed for both forward and reverse orientations of the orifice plates. In each case, the discharge coefficient was calculated based on the pressure drop across the plate, and the results were compared with the values provided by ISO 5167-2 [3] for the forward orientation, and with the values from the Gas Research Institute (GRI) report [2] for the reverse orientation.

3.1.1 NEL Geometry

To capture the as found condition of the orifice plates, a high accuracy laser scan was undertaken by Physical Digital. The deviation between the Standard Tessellation Language (STL) surface and the reversed engineered CAD is shown in Figure 3.

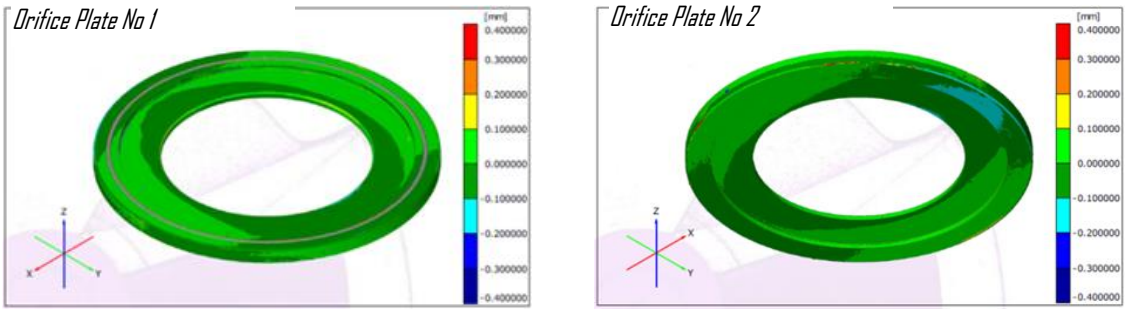

Figure 3 – Surface Comparison to CAD View

The reverse engineered model obtained from the laser scan shows in Figure 4 the 3D CAD representation of the orifice plate with the sharp edge and bevel.

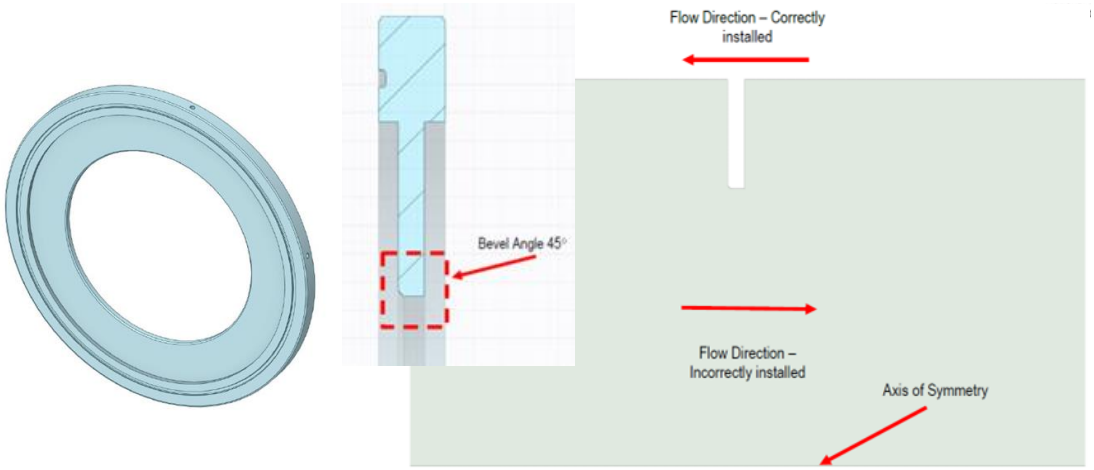

Figure 4 – NEL 2D and 3D Model Geometry: Quarter Symmetry Model

To reduce the computational time, symmetry was exploited, and a quarter symmetry model was used. As the drawings of the piping configuration and the internal dimensions of the pressure tappings were not available, they were omitted from the model to support symmetry.

3.1.2 NEL Mesh

The unstructured polyhedral mesh, with local refinement (i.e. smaller cell size) around the sharp edge of the orifice plate was used for the ideal cases. A high level of refinement has been used in the vicinity of the orifice plate. This is critical because the pressure drop measured is driven primarily by separation which occurs at the sharp edge. A refined boundary layer mesh has been applied throughout the model to ensure that the values of y+ throughout the domain are appropriate for the use of wall functions.

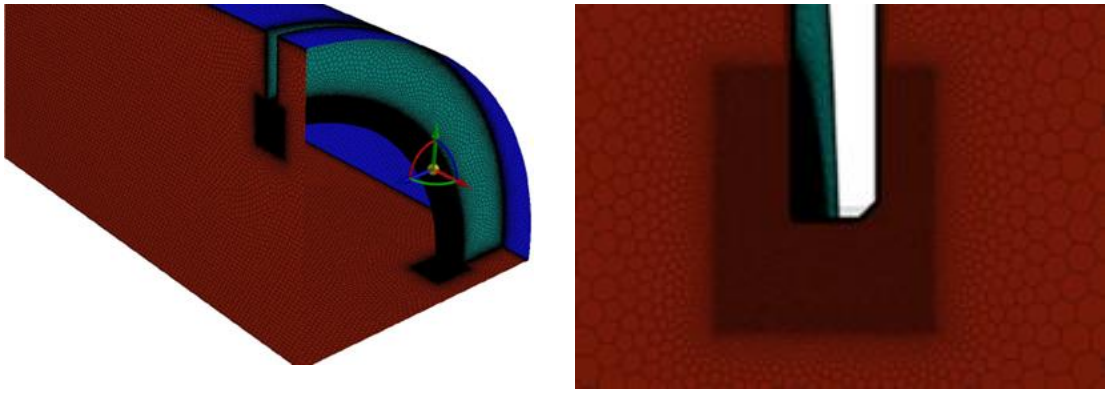

Figure 5 – NEL Mesh Grid

A mesh independence study was performed for only one orifice plate installed in the correct orientation at three flow rates. The difference of 0.12 % was found with the elements size refinement from 0.4 mm to 0.2 mm. Despite mesh independence being achieved using 0.4 mm, the finer mesh of 0.2 mm was used for all simulations. This resulted in a mesh size of approximately 40 million cells for each model.

3.1.3 NEL Model Setup

A steady state CFD simulation was performed and a k-ε realisable turbulence model was used due to its effectiveness in handling separated flows, which are common in orifice plates. Laminar and turbulent flows are significantly affected by the presence of walls and therefore

adequate refinement is required to capture the large gradients between the bulk flow and the wall. The enhanced wall treatment function was used to model this large gradient and is applicable for a wide range of Reynolds numbers.

3.1.4 NEL Boundary Conditions

The boundary conditions that were applied to the forward and reversed orifice plate models are provided in Table 5.

Table 5 – Boundary Conditions and Fluid Properties for NEL CFD Model

Case	Inlet Velocity, m/s	Density, kg/m^3	Dynamic Viscosity, cP	Reynolds Number	Mass Flow Rate, kg/s
Low	4	49.38	0.012	7,095,190	28.98
Medium	8	49.38	0.012	14,190,381	57.96
High	15	49.38	0.012	26,606,964	108.67

3.1.5 NEL CFD Model Validation

The CFD model was validated for the forward orientation against the ISO 5167-2 standard [3], and for the reverse orientation against data published in the GRI Report [2]. This was done to assess how accurately the CFD process captures the changes in the discharge coefficient when an orifice plate is reversed.

The discharge coefficients for the forward orientation, calculated from the CFD simulation results obtained for both orifice plates, matched the values derived from the ISO 5167-2 standard, with an agreement of up to 0.9 %, and the best match being 0.1 % at the lowest flow rate, as shown in Table 6.

Table 6 – NEL CFD Model Validation in Forward Orientation

Orifice Plate	Case	ISO 5167-2 [3] Discharge Coefficient	CFD Discharge Coefficient	Discharge Coefficient Error: CFD vs ISO 5167-2, %
No 1	Low	0.59767	0.59706	-0.10266
	Medium	0.59701	0.59377	-0.54306
	High	0.59653	0.59119	-0.89592
No 2	Low	0.59768	0.59496	-0.4543
	Medium	0.59702	0.59386	-0.52933
	High	0.59654	0.59133	-0.87361

The percentage relative shift in discharge coefficients for the forward and reverse orientations, as calculated from the CFD simulation results performed for four experimental test points from the GRI Report, matched the values provided in the report to within 1 %, as shown in Table 7.

Table 7 – NEL CFD Model Validation in Reverse Orientation

Test Point Forward	Test Point Reverse	GRI Report [2] Shift in Discharge Coefficient, %	CFD Forward Discharge Coefficient	CFD Reverse Discharge Coefficient	CFD Shift in Discharge Coefficient, %
F082600.010	F082600.030	**13.78**	0.60969	0.69509	**14.01**
F082600.015	F082600.035	**13.69**	0.61108	0.69597	**13.89**

This validation confirmed that the simulation results for both orientations, using the proposed model, fall within the 1 % limit and can be considered technically robust.

3.1.6 NEL Simulation Results

All results refer to the maximum flowrate of 108.67 kg/s. Contours of static pressure and velocity for both forward and reverse orientation are shown in Figure 6 and Figure 7. It can be observed that when the orifice plate is installed in the reverse orientation the velocity profile is different since the separation occurs from the bevel rather than from this sharp edge. This has a significant effect on the pressure drop and therefore contributes to a flow measurement error.

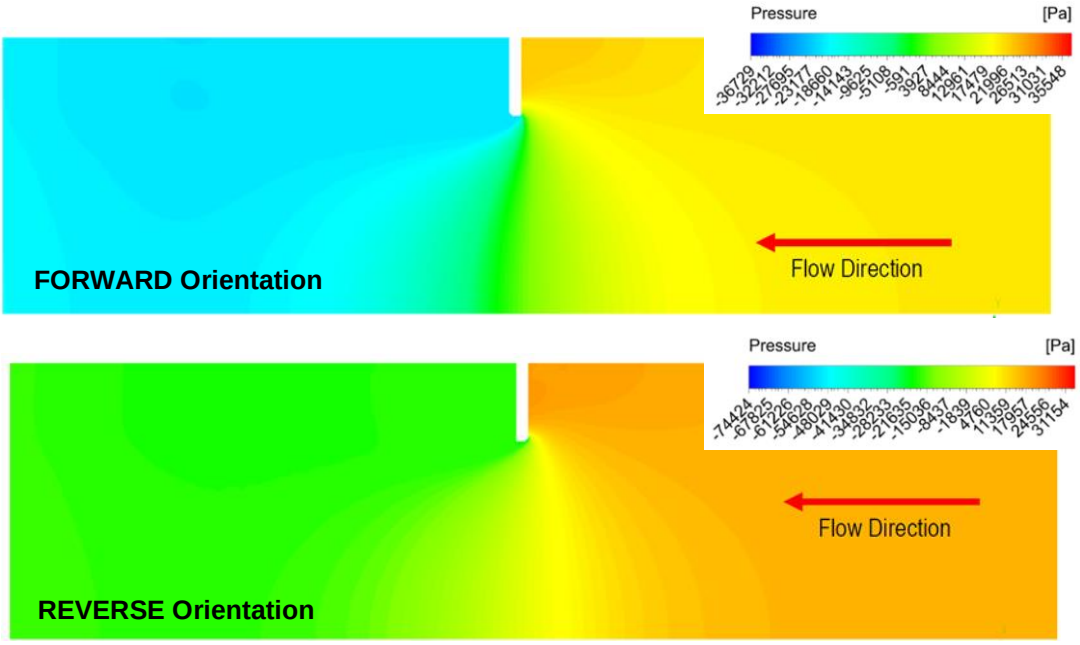

Figure 6 – NEL Static Pressure Contours for Forward and Reverse Orientation

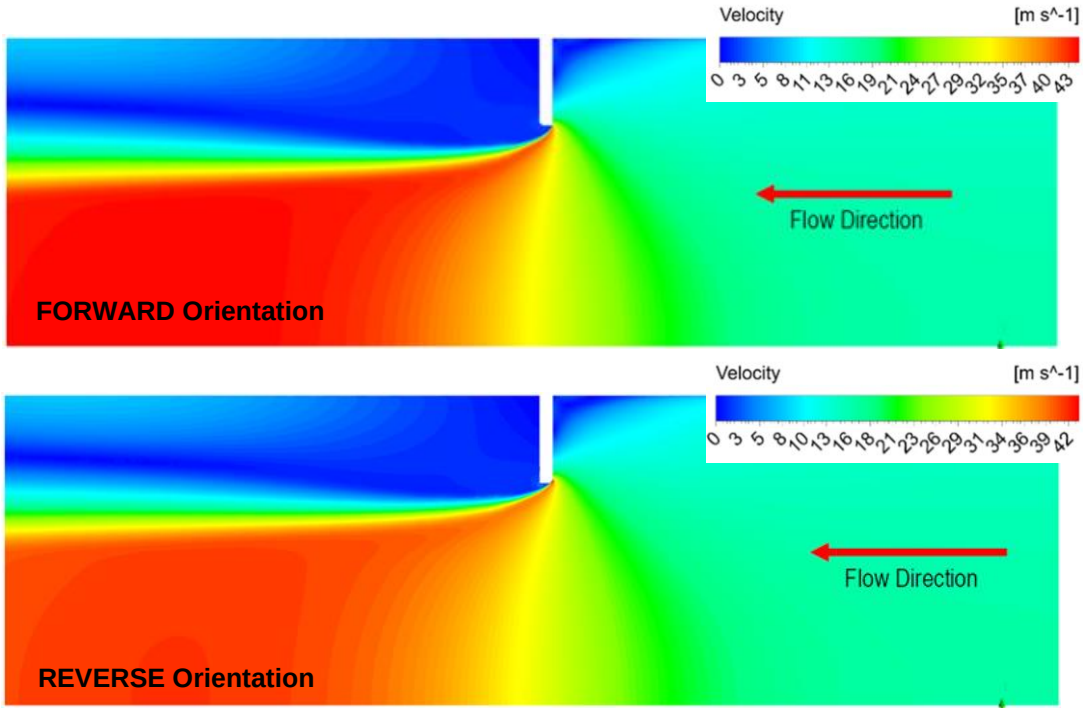

Figure 7 – NEL Velocity Contours for Forward and Reverse Orientation

The CFD simulations confirmed changes in the discharge coefficient for both plates when installed in the reverse orientation, as shown in Table 8. Plate No 1 requires a larger correction, not exceeding 7.37 %, while plate No 2 requires a smaller correction, not exceeding 5.64 %. In both cases, the CFD results indicate that the reverse orientation causes a systematic undermeasurement, necessitating the application of a correction factor to adjust the reported flow rates. Furthermore, in both cases, the computed shift in the discharge coefficient is not constant and exhibits non-linear behaviour across the range of modelled Reynolds numbers.

Table 8 – NEL Computed Discharge Coefficients and Measurement Error

Orifice Plate	Case	CFD Forward Discharge Coefficient	CFD Reverse Discharge Coefficient	Shift in Discharge Coefficient, %
No 1	Low	0.59706	0.63556	6.45
	Medium	0.59377	0.63465	6.88
	High	0.59119	0.63475	7.37
No 2	Low	0.59496	0.62663	5.32
	Medium	0.59386	0.62559	5.34
	High	0.59133	0.62469	5.64

3.2 CFD Approach by Emerson (SUSU)

Emerson (SUSU) also employed CFD simulations, using both ANSYS Fluent and ANSYS CFX. The key difference between Emerson's approach and NEL's was the use of the **k-ω Shear Stress Transport (SST) turbulence model**. This model is known for its predictive capability of boundary layers and separation, making it well-suited for predicting the flow behaviour in the vicinity of the orifice plate.

Similar to the NEL study, Emerson used three Reynolds numbers for simulations, but the range was significantly reduced to account for the field flow conditions. The geometry of the plates was based on calibration certificates, and a **structured hexahedral mesh** with refinements near the orifice edge was used to capture the sharp pressure and velocity gradients caused by the flow separation at the plate. The mesh independence was checked.

The simulations were performed for both forward and reverse orientations of the orifice plates. In each case, the discharge coefficient was calculated based on the pressure drop across the plate, and the results were compared to the values provided by ISO 5167-2 [3] for the forward orientation. To validate the model in reverse orientation, the case described in paper [1] was remodelled and the shift in discharge coefficient was compared against the reported results.

3.2.1 Emerson (SUSU) Geometry

Figure 8 illustrates the computational domain. The upstream length of 23D defined by the flange connection is selected for the modelling. The following pipework elements are not considered in the model: thermowell, upstream valve, and upstream 45-degree bend.

For the modelling of the forward orientation of the orifice plate the flow from left to right is considered, and for the reverse orientation the flow direction is swapped to from right to left. Therefore, the downstream length is set to 23D as well, and the overall length of the computational domain in the pipe axial direction forms 46D plus the orifice plate thickness 'E'.

The flow through the orifice plate is assumed steady and axisymmetric to reduce the number of mesh elements and consequently computational time. Therefore, the model is limited by the axis of rotational symmetry along the pipe. The 3D model is obtained by rotating the 2D geometry by the rotation angle (3° for CFX and 7.5° for Fluent), which represents the default value preset in the solvers.

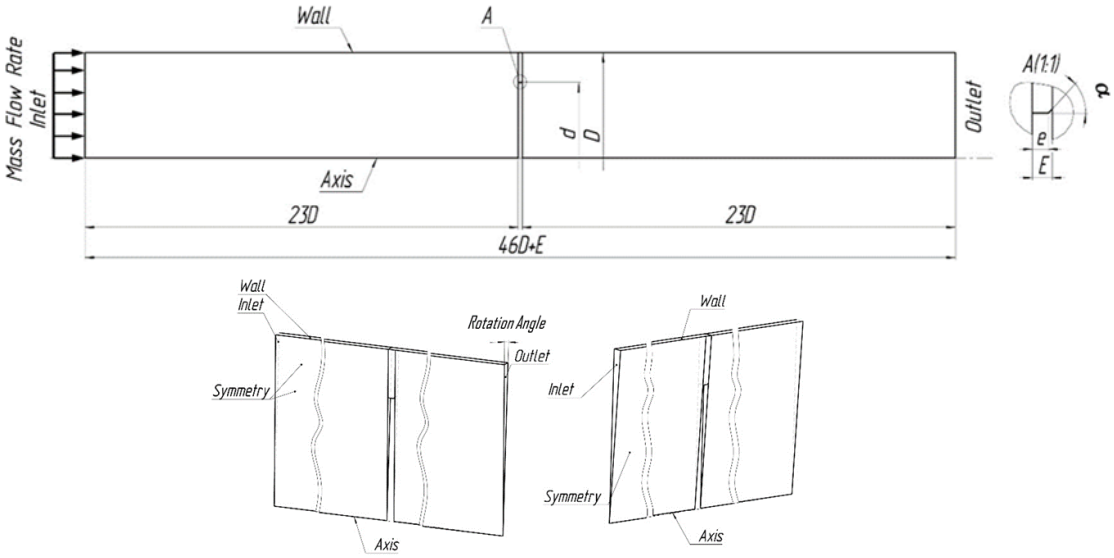

Figure 8 – SUSU 2D and 3D Symmetry Model Geometry

3.2.2 Emerson (SUSU) Mesh

The structured hexahedral mesh used for CFD simulation is shown in Figure 9 around the orifice plate edge. The mesh consists of nearly 994,000 nodes and 0.5 million hexahedral elements, arranged in a single layer, with prismatic elements along the axis of rotation. The wall-adjacent elements form the layer with the element size set by using the non-dimensional wall distance parameter y+<100. The mesh independence study was performed by increasing number of elements from 0.5 million to 1.1 million. With an improvement in the discharge coefficient prediction of 0.17 %, the simulation time increased from 2 hours to 8.5 hours. Therefore, it was agreed to accept the mesh of 0.5 million elements for further simulations.

The region upstream and downstream of the plate is filled with square elements; this ensured that the element structure surrounding the plate is the same for both the forward and reverse orientations. The size of these square elements is 0.1 mm, giving 22 elements along the orifice-edge and 70 along the bevel. Outside the orifice plate region, the grid was expanded to the inlet and outlet planes to optimise the count of the elements.

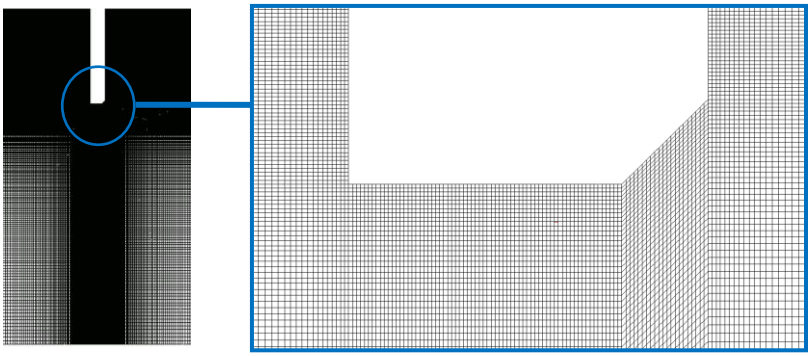

Figure 9 – SUSU Mesh Grid

3.2.3 Emerson (SUSU) Model Setup

To perform the numerical simulation, the Reynolds-Averaged Navier-Stokes equations (RANS) are chosen as a mathematical model. The RANS-based turbulence model k-ω SST [5] is selected for both solvers.

The k-ω SST turbulence model is suitable for modelling of complex turbulent flows. It is adaptive to the wide range of the y+ distance parameter (from 0 to 100) and accurately predicts the point of flow separation and the area of flow separation zones at adverse pressure gradients. The k-ε models are not as good as k-ω models at y+ values close to zero what is specific for zero velocity condition on the walls.

The k-ω SST turbulence model is a two-equation eddy-viscosity model. The shear stress transport (SST) formulation combines the best of two models. The use of a k-ω formulation in the inner parts of the boundary layer makes the model directly usable all the way down to the wall through the viscous sub-layer. The SST formulation also switches to a k-ε behaviour in the free-stream and thereby avoids the common k-ω problem that the model is too sensitive to the inlet free-stream turbulence properties.

The discretization methods used in the model are second order for the momentum and mass equations, and first for the turbulence equations. The convergence of the solution for scaled residuals is set at 10^{-5}.

3.2.4 Emerson (SUSU) Boundary Conditions

The boundary conditions that were applied to the forward and reversed orifice plate models are provided in Table 9. The mass flow rate is set as a boundary condition at the inlet along with the evenly distributed velocity profile. The RANS equations with standard no-slip adiabatic boundary conditions on the smooth walls and a zero-gradient boundary condition at the outlet are established.

Table 9 – Boundary Conditions and Fluid Properties for SUSU CFD Model

Case	Inlet Velocity, m/s	Density, kg/m³	Dynamic Viscosity, cP	Reynolds Number	Mass Flow Rate, kg/s
Low	3.2530	50.33	0.01204	5,878,987	24.03
Medium	4.9502	50.33	0.01204	8,946,285	36.57
High	6.6474	50.33	0.01204	12,013,583	49.11

3.2.5 Emerson (SUSU) CFD Model Validation

Similarly to the NEL study, the SUSU CFD model was validated for the forward orientation against the ISO 5167-2 standard [3], but for the reverse orientation it was validated against the modelling data published in the NSFMW paper [1], which assessed the measurement error for the orifice plate installed in the reverse orientation on the Judy platform.

As in the NEL study, the SUSU CFD results for the forward orientation, presented in Table 10, closely match the discharge coefficients calculated using the ISO 5167-2 standard [3].

Table 10 – SUSU CFD (CFX / Fluent) Model Validation in Forward Orientation

Orifice Plate	Case	ISO 5167-2 [3] $C \cdot \varepsilon$	CFD (CFX/Fluent) $C \cdot \varepsilon$	Error: CFD (CFX/Fluent) vs ISO 5167-2, %
No 1	Low	0.5978	0.5965 / 0.5962	-0.23 / -0.27
	Medium	0.5973	0.5951 / 0.5950	-0.37 / -0.38
	High	0.5969	0.5939 / 0.5942	-0.50 / -0.44
	Re=14.2·10⁶	0.5966	- / 0.5938	- / -0.47
	Re=26.6·10⁶	0.5949	- / 0.5920	- / -0.49
No 2	Low	0.5978	0.5965 / 0.5963	-0.22 / -0.26
	Medium	0.5973	0.5951 / 0.5951	-0.36 / -0.37
	High	0.5969	0.5939 / 0.5943	-0.50 / -0.43
	Re=14.2·10⁶	0.5966	- / 0.5939	- / -0.46
	Re=26.6·10⁶	0.5949	- / 0.5921	- / -0.47

The discharge coefficients calculated from the CFD simulation results showed an agreement of up to 0.5 % with the standard, as presented in Table 10 for both solvers, CFX and Fluent. This error is within the uncertainty of 0.7 % specified in the standard for the discharge coefficients in the range $0.6 < \beta \leq 0.75$. The errors obtained by both solvers are comparable and appear to be lower at lower flow rates (Reynolds numbers).

The results of the CFD simulations provided by SUSU and NEL are compared in Figure 10. At lower Reynolds numbers, the simulations demonstrate good agreement with the standard, as well as consistency between different CFD models, with discrepancies of no more than 0.3 %, all follow the same trend. However, as Reynolds number increases, the error also rises, and the discrepancies between the results from the two CFD ITEs become more apparent. The modelling at high Reynolds numbers was initially not performed by SUSU but was added later during the results comparison stage.

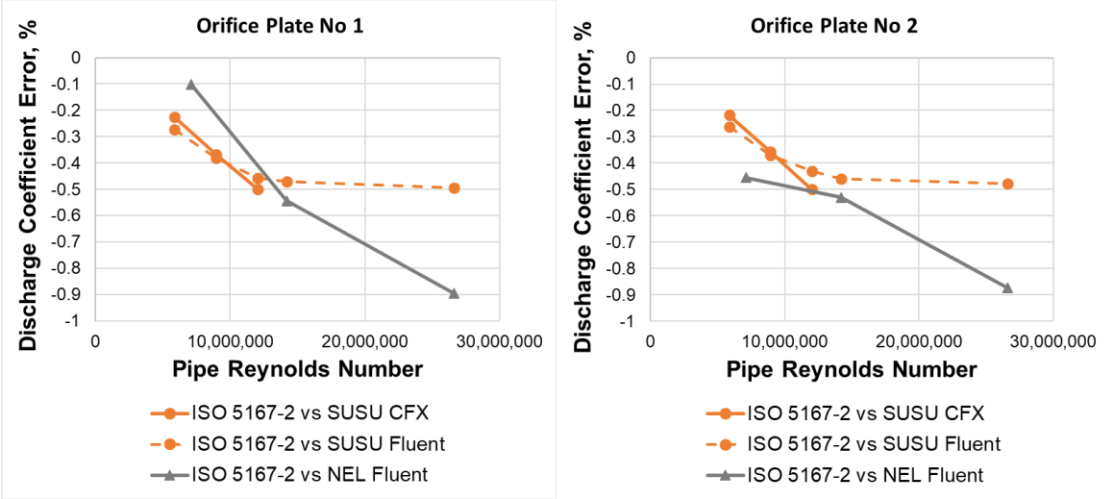

Figure 10 – Comparison of ISO 5167-2 and CFD Results for Discharge Coefficient

For validation of the model in the reverse orientation, the CFD results obtained using the SUSU CFD model setup were compared against the modelling data published in the NSFMW paper [1] for Judy Orifice Plate. The differences in the model geometry, grid, setup, and boundary conditions are summarised in Table 11. The plate and pipe dimensions, along with the process conditions, are as detailed in the paper [1]. In particular, $Re_D=12.08 \cdot 10^6$, $\beta=0.5802$, $e=4.5$, $b=5.02$, $b/d=0.033$, $b/E=0.53$.

Table 11 – Differences in Model Setup for Judy Orifice Plate

Parameter	**NEL**, NSFMW Paper [1]	**Emerson (SUSU)**
CFD Solver Name	ANSYS Fluent	ANSYS CFX, ANSYS Fluent
Turbulence Model	realisable k-ε [7]	k-ω SST [5]
Mesh Grid	1.05 mm size of elements 8 elements along the orifice-edge 14 elements along the bevel	0.1 mm size of elements 22 elements along the orifice-edge 70 elements along the bevel
Number of elements	130,000	500,000
Upstream and Downstream Length	3D	23D
Inlet Boundary Conditions	Fully developed flow	Mass flow rate and evenly distributed velocity across pipe

Table 12 shows the results of the computations performed using CFX and Fluent solvers, compared to one of the cases provided in the paper [1].

Table 12 – SUSU CFD Model Validation in Forward Orientation for Judy Orifice Plate

Orifice Plate	ISO 5167-2 [3]	Source	CFD	Error: CFD vs ISO 5167-2, %
Judy Platform	C = 0.6041 $C \cdot \varepsilon$ = 0.6028	Paper [1]	C = 0.5990	-0.84
		SUSU CFX	$C \cdot \varepsilon$ = 0.6002	-0.43
		SUSU Fluent	$C \cdot \varepsilon$ = 0.5995	-0.55

For the forward orientation, the best match with the ISO 5167-2 standard [3] is observed in the CFX computation result, with an error of -0.43 %, which falls within the uncertainty of 0.5 % specified in the standard for the discharge coefficients in the range $0.2 \leq \beta \leq 0.6$.

For the reverse orientation, data from the offshore verification trials for Judy Orifice Plate indicated a correction in discharge coefficient of approximately 19.4 % as detailed in Table 13. The Fluent computation result closely aligns with the offshore verification trials, showing a correction of 17.83 %, as illustrated in Figure 11. In this figure, the CFX and Fluent computational results are plotted alongside the data published in the paper [1].

Table 13 – SUSU CFD Model Validation in Reverse Orientation for Judy Orifice Plate

Orifice Plate	Source	CFD Forward	CFD Reverse	Error, %	Offshore Verification Error, %	CFD Difference from Offshore Verification, %
Judy Platform	Paper [1]	C = 0.5990	C = 0.7289	21.67	19.4	2.27
	SUSU CFX	$C \cdot \varepsilon$ = 0.6002	$C \cdot \varepsilon$ = 0.7009	16.77		-2.63
	SUSU Fluent	$C \cdot \varepsilon$ = 0.5995	$C \cdot \varepsilon$ = 0.7064	17.83		-1.57

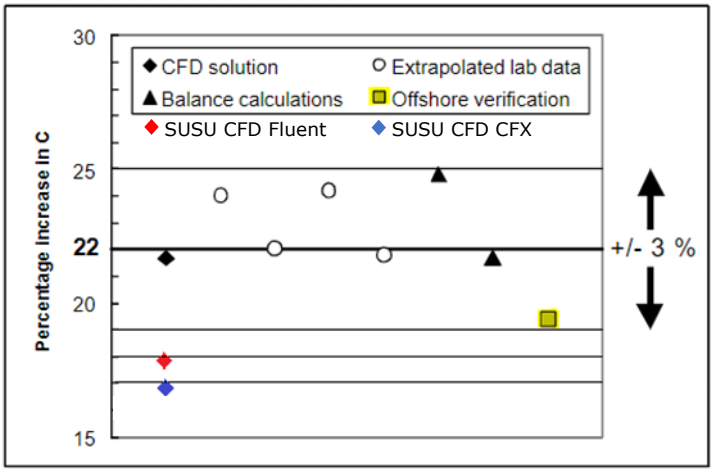

Figure 11 – Summary of Results for Judy Orifice Plate

This validation confirms that the simulation results for both orientations, using the proposed CFD model, are within the 0.5 % uncertainty limit for the forward orientation (see Table 10), and within 3 % limit for the reverse orientation (see Table 13). The obtained errors can be deemed satisfactory, and the proposed CFD model can be regarded as technically robust.

3.2.6 Emerson (SUSU) Simulation Results

All results presented for a typical (medium) flowrate of 36.57 kg/s. Figure 12 illustrates the velocity field, flow lines, and the velocity profile along the wall at the 6D, 8D, and 10D locations, both upstream and downstream of the orifice plate, and at pressure tappings P1 and P2. The theoretical velocity profile for a smooth wall (denoted as 'Theory' in the graphs legend) is defined by the logarithmic law [6]. Upstream of the orifice plate, the velocity profile

is closely aligned with the logarithmic law. Downstream of the orifice plate, the velocity profile is fully recovered by 10D and conforms to the logarithmic law for both forward and reverse orientations. In the forward orientation, the velocities are higher at P1 and P2, but lower at the 6D, 8D, and 10D locations downstream.

FORWARD Orientation

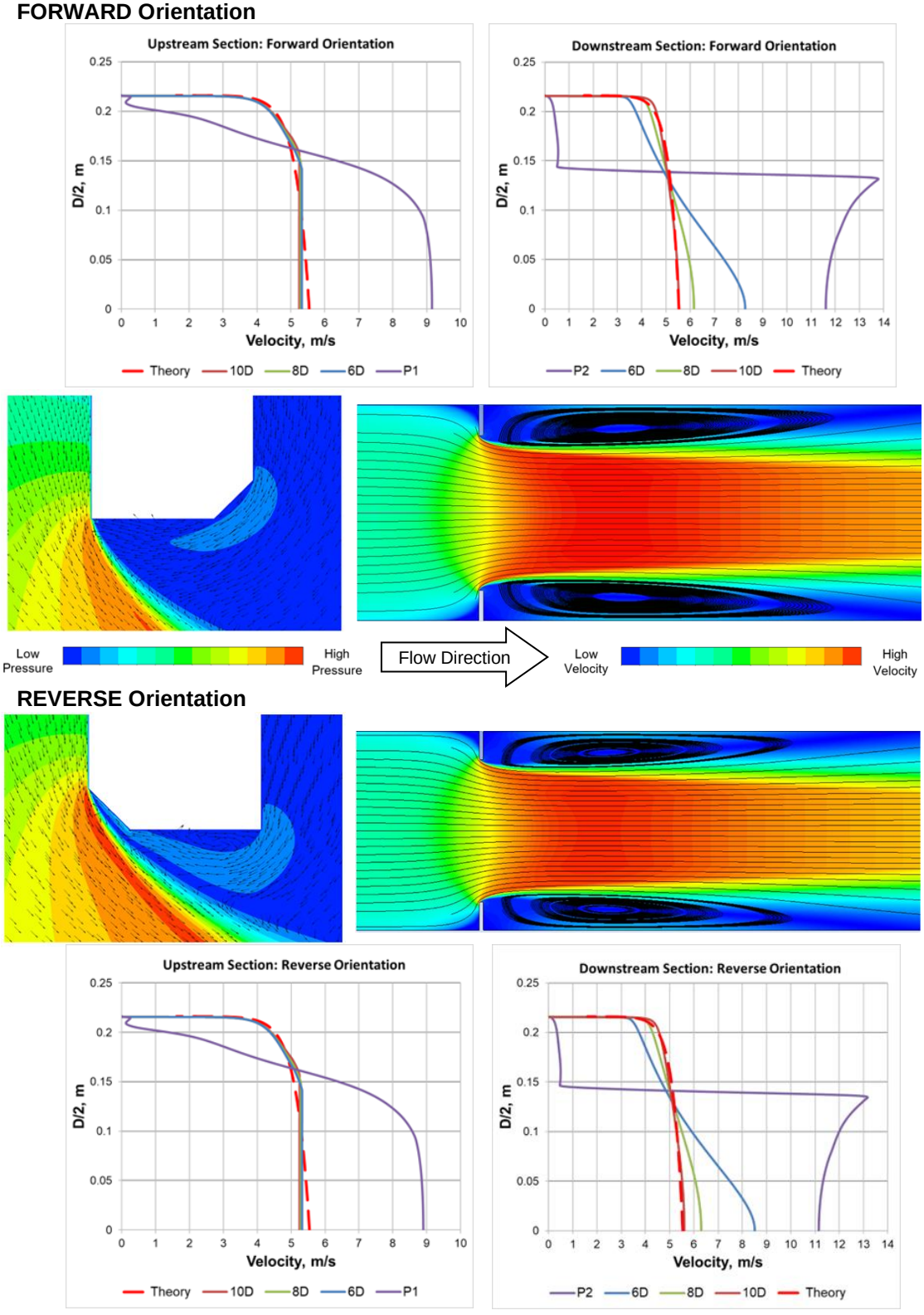

Figure 12 – SUSU Velocity Field and Flow Lines for Forward and Reverse Orientation

The separation around the orifice plate edge at forward and reverse orientations is also shown in Figure 12. The sharp edge of the orifice plate, in the forward orientation, forces the flow to separate and turn abruptly, ensuring that the orifice plate geometry (thickness and bevel angle) does not significantly affect the flow meter operation. However, in the reverse orientation, the orifice plate geometry (thickness and bevel angle) starts having a significant impact on the flow pattern, which can be compared to a nozzle. In this scenario, the flow is directed by the 45° bevel of the orifice plate and remains attached to the bevel surface, forming several zones of flow separation along the surface.

Figure 13 shows the pressure profile along the upstream and downstream walls of the orifice plate flow meter. Both the upstream and downstream pressure profiles are illustrated for forward (solid line) and reverse (dashed line) orientations at three flow rates: low, medium, high (refer to Table 9). The pressure on the wall 'Px' is referred to the upstream pressure 'Pup', and pressure profiles show the difference (Px-Pup) in pascals (Pa). The pressure tappings, 6D, and 8D downstream locations are marked on the graph by vertical dashed lines.

The pressure profiles in both orientations exhibit a similar shape. A region of relatively constant pressure occurs just downstream of the plate, where the downstream pressure tapping is located. Within this region, the pressure decreases to its minimum, but then gradually recovers as it approaches the 6D plane. The pressure profiles both upstream and downstream resemble the approximate profiles of ISO 5167-2 provided in Figure 14, where 1 and 2 correspond to the locations of the pressure tappings (P1 and P2).

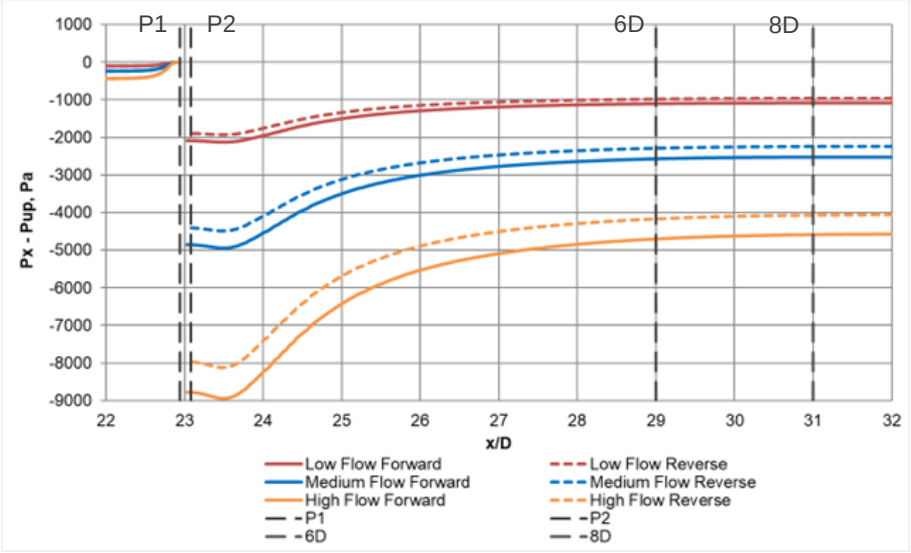

Figure 13 – Static Pressure Upstream and Downstream of Orifice Plate in Forward and Reverse Orientation

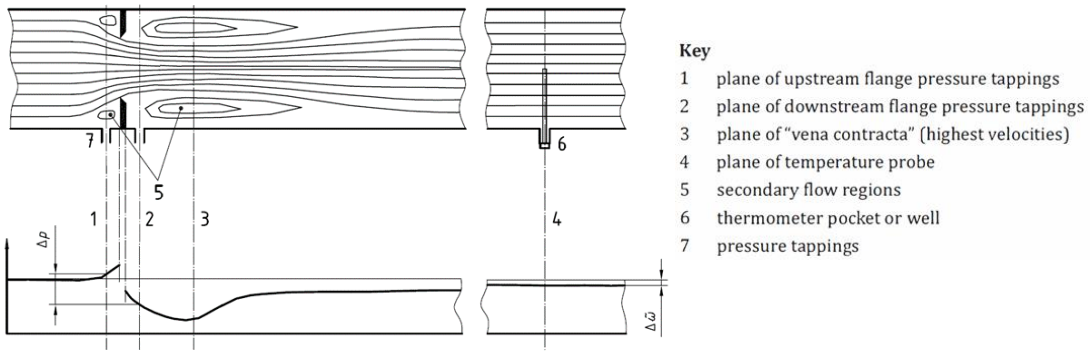

Figure 14 – Approximate Profiles of Flow and Pressure in an Orifice Plate

The CFD simulations confirmed changes in the discharge coefficient for both plates when installed in the reverse orientation, as shown in Table 14. Plate No 1 requires a larger correction, not exceeding 5.70 %, while plate No 2 requires a smaller correction, not exceeding 4.15 %. The difference between the Fluent and CFX solvers is less than 0.8 %, with Fluent predicting a lower correction. This difference can be attributed to the reproducibility of the CFD simulations.

Table 14 – SUSU (CFX / Fluent) Computed Discharge Coefficients and Measurement Error

Orifice Plate	Case	CFD (CFX/Fluent) Forward Discharge Coefficient	CFD (CFX/Fluent) Reverse Discharge Coefficient	Shift in Discharge Coefficient (CFX/Fluent), %
No 1	Low	0.5965 / 0.5962	0.6305 / 0.6257	5.70 / 4.95
	Medium	0.5951 / 0.5950	0.6283 / 0.6243	5.58 / 4.92
	High	0.5939 / 0.5942	0.6269 / 0.6234	5.56 / 4.91
No 2	Low	0.5965 / 0.5963	0.6213 / 0.6180	4.15 / 3.64
	Medium	0.5951 / 0.5951	0.6194 / 0.6166	4.07 / 3.62
	High	0.5939 / 0.5943	0.6179 / 0.6158	4.04 / 3.61

Emerson (SUSU) CFD simulations produced results similar to those of NEL, confirming an undermeasurement when the plates are in reverse orientation. As shown in Figure 15, SUSU's predicted measurement errors are lower and more stable than NEL's, particularly for Plate No. 1, where the difference is more pronounced.

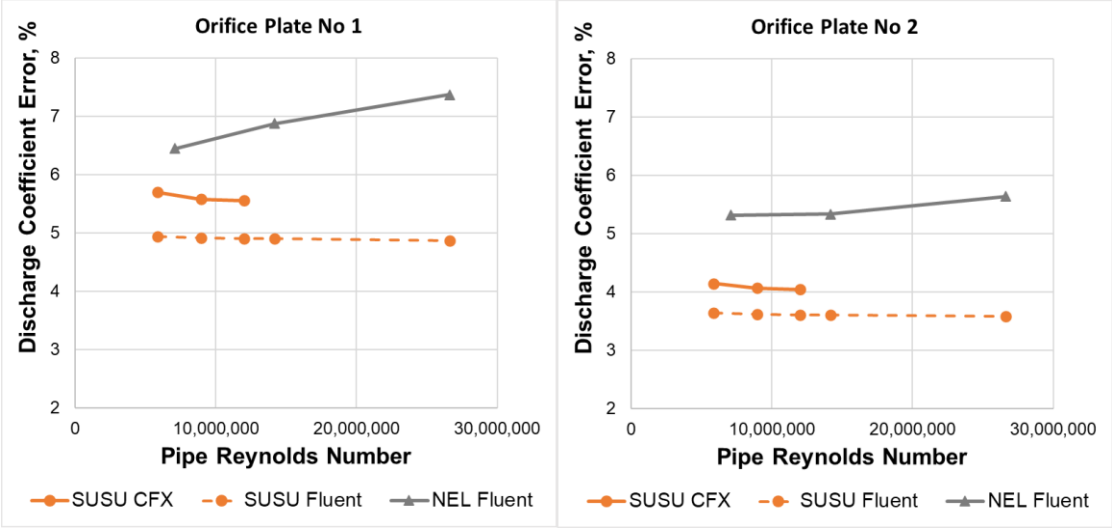

Figure 15 – Comparison of CFD Results for Discharge Coefficient Error

The discrepancy between the SUSU and NEL results increases with rising Reynolds numbers, though it does not exceed 2.5 %. The variation observed among the three CFD simulation results is significant from a mismeasurement perspective, making it necessary to conduct experiments to determine the correct adjustment. Experimental validation is essential to confirm which correction should be applied for achieving accurate results.

4 EXPERIMENTAL FLOW TESTING USING CLAMP-ON USM

4.1 Flow Test Setup and Methodology

To determine the measurement error caused by the reverse orientation of the orifice plates and to validate the previously obtained CFD simulations, a flow test was proposed and

conducted. The test was carried out by i-Vigilant Technologies Limited using a clamp-on ultrasonic flow meter (USM), installed 5.2D upstream of the orifice plate flow meter, as shown in Figure 16. The orifice meter stream has 49D of upstream straight length meaning there is approximately 44D of upstream stream length before the USM. For the testing, it was assumed that the pressure, temperature, and density at the USM are as measured by the orifice plate meter.

The primary objective was to measure the flow rate for both the forward and reverse orientations of the orifice plates, and to compare these results with the CFD simulations performed by NEL and Emerson (SUSU).

Figure 16 – Clamp-on USM Installation 5.2D Upstream to Orifice Plate Flow Meter

Ultrasonic meters are non-intrusive instruments used to measure flow velocity by transmitting sound waves through a fluid. One of the key advantages of a clamp-on meter is that it can be installed without interrupting the flow or requiring any modifications to the piping system. A portable, clamp-on ultrasonic flow meter available at the time of testing was the Fluxus G608 from Flexim, equipped with GLK1NH3 transducers. The flow meter was set to operate on a single diametral path, where ultrasonic signals are transmitted diagonally across the pipe diameter, as shown in Figure 17. The USM was configured based on measurements of the pipe wall thickness and its circumference. The USM settings are listed in Table 15.

Table 15 – USM Configuration Parameters

Parameter	**Units**	**Value**
Pipe Wall Thickness	mm	12.3
Outer Diameter	mm	464.73
Transducer Distance	mm	22
Nominal Transducer Frequency	Hz	500,000
Fluid	-	Natural Gas (90 % Methane)
Pipe Material	-	Carbon Steel
Damping	s	10
Data Logger Averaging	-	Enabled
Data Logger Storage Rate	s	30

Regrettably, the transducers used for the test were outside the manufacturer's recommendation for this pipe, as the GLK transducers are only suitable for wall thicknesses between 5 mm and 9 mm. Furthermore, these transducers operate with a single-channel measurement in direct mode, which makes them sensitive to any crossflows or fluctuations in the flow profile. A GLH/GRH transducer with a frequency of 300,000 Hz would have been a

more appropriate option for this test, allowing for a double-channel setup in reflex mode, as shown in Figure 17, resulting in a more stable measurement. However, waiting for the more suitable transducers could have resulted in the cancellation of the test altogether, so a compromise was accepted to proceed with the flow test.

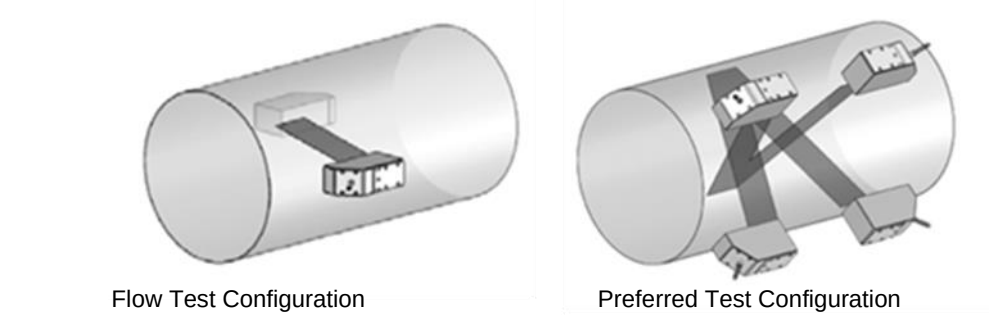

Flow Test Configuration Preferred Test Configuration

Figure 17 – Transducer Orientation

The flow tests were conducted over multiple days, with the orifice plates installed in both forward and reverse orientations. Each flow test ran for 4 hours, during which stability was monitored to ensure sufficient data was acquired to establish an accurate standard volume for comparing the orifice plate flow meter with the clamp-on USM.

Due to the anticipated systematic errors in the USM, during the initial test it was run in series with the orifice plate No 1 installed in the forward orientation to determine a meter factor (MF). As an additional baseline check and to confirm the reproducibility of the USM, the orifice plate No 2 was tested in the forward orientation as well.

During the flow test, the data logging was critical to ensure accurate measurement. Data from the orifice system was logged using the onsite monitoring application, which recorded the measured parameters (differential pressure, pressure, temperature, instantaneous standard volume flow rate, standard volume totals) along with gas quality information, storing it in comma-separated value (CSV) files. The storage rate was dictated by the 7-minute cycle time of the gas chromatograph (GC). Offline compressibility and density calculations, following AGA8, were performed for an ISO 5167-2 calculation check and to convert the USM actual volume flow rate to standards volume flow rate.

The Fluxus G608 transmitter is battery-operated and supports local data logging at a much higher rate and was configured to store averaged data every 30 seconds. After the completion of each flow test, the transmitter was connected to a laptop, and the logged data downloaded and stored in CSV files.

4.2 Flow Test Results

The first set of tests were conducted with the orifice plate No 1 at a throughput of approximately 160,000 Sm^3/h. When the plate was installed in the forward orientation, the meter factor for the clamp-on USM was determined to be 0.9719. This meter factor was then applied to all subsequent measurements. After the initial test, the orifice plate was removed, reinstalled in the reverse orientation, and the flow test was repeated at the same flow rate.

Figure 18 illustrates the flow test results for both forward and reverse orientations in terms of standard volume, where several trends are shown. The blue, grey, and orange trends represent the orifice system flow rate measurement results: the flow rate based on the total (blue), the average flow rate of all instantaneous readings from the start of the test to the point of plotting (grey), and the instantaneous readings themselves (orange). The average flow rate of the test was calculated based on the totaliser (blue trend) and the instantaneous measured flow rates (orange trend). The difference between these two figures was found to be -0.23 % for the forward orientation and 0.14 % for the reverse orientation. Given the

fluctuating flow rates and data logging frequency, this variation was considered to be within a reasonable resolution.

The yellow trend in Figure 18 represents the meter-factor-corrected readings from the USM. As would be expected, the USM and orifice plate results are in close agreement after applying the meter factor for the forward orientation flow test. The yellow trend for the reverse orientation flow test consistently shows higher readings than the orifice plate, confirming that the orifice plate undermeasures flow in reverse orientation. The error was calculated as **5.814 %**.

FORWARD Orientation

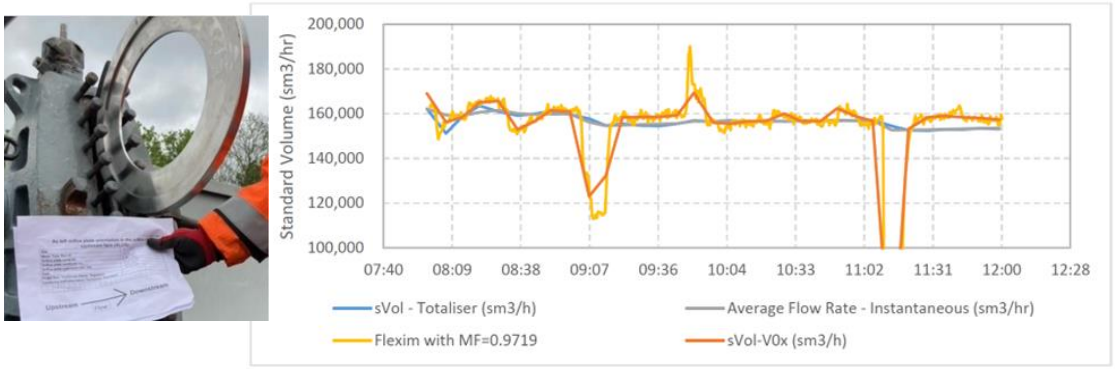

REVERSE Orientation

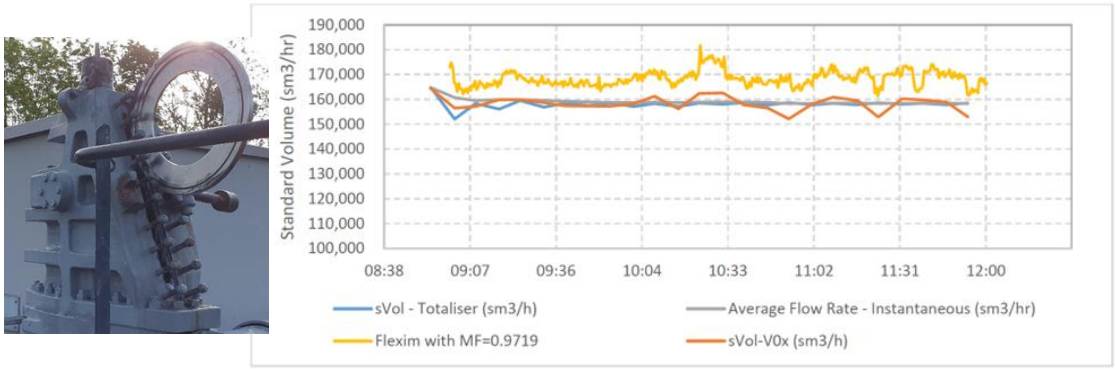

Figure 18 – Orifice Plate No 1 Flow Test

The second set of tests was conducted with the orifice plate No 2 at a throughput of approximately 160,000 Sm^3/h. When the second plate was installed in the forward orientation, the difference between the USM and the orifice plate was established as -0.025%, demonstrating excellent reproducibility from the first flow test. After this, the orifice plate was removed, reinstalled in the reverse orientation, and the flow test was performed at the same flow rate.

The flow test results for both forward and reverse orientations are illustrated in Figure 19, in terms of standard volume, where several trends are shown. The colour coding follows the same convention as in the previous test. The average flow rate of the test was calculated from both the totaliser (blue trend) and the instantaneous measured flow rates (orange trend). The difference between these two figures was found to be -0.27 % for the forward orientation and -0.2 % for the reverse orientation.

The yellow trend in Figure 19 represents the meter-factor-corrected readings from the USM. The USM and orifice plate results are in close agreement for the forward orientation flow test. The yellow trend for the reverse orientation flow test consistently shows higher readings than the orifice plate, confirming that the orifice plate undermeasures flow in reverse orientation. The error was calculated as **4.324 %**.

FORWARD Orientation

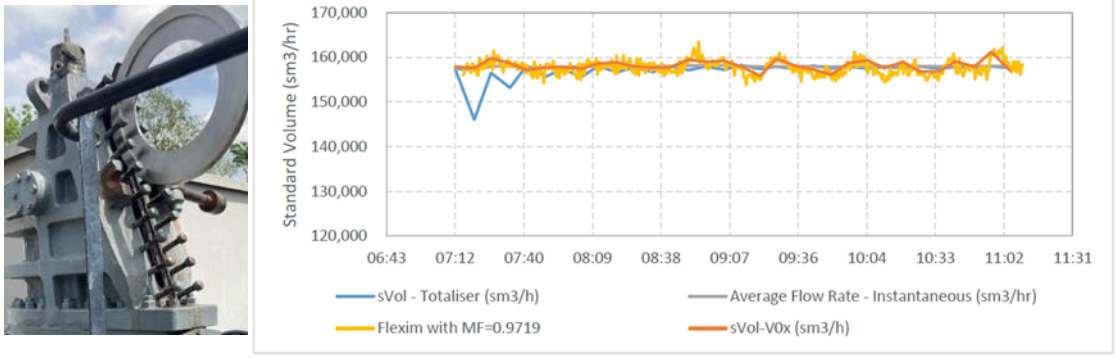

REVERSE Orientation

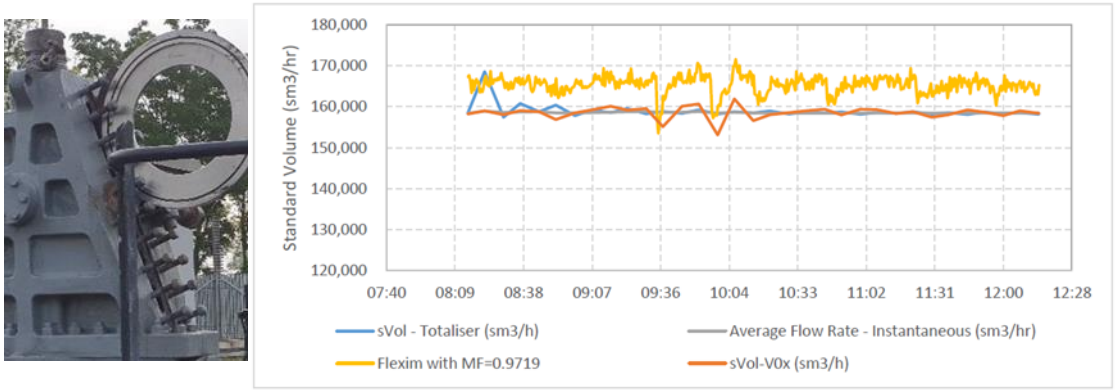

Figure 19 – Orifice Plate No 2 Flow Test

4.3 Flow Test and CFD Comparison

A summary of the results is presented in Table 16. The flow test carried out on orifice plate No 1 in the forward orientation was used to establish a meter factor. This factor compensates for possible systematic errors (transducer alignment, pipe dimensions, etc.) and was applied to the tests conducted in the reverse orientation. Orifice plate No 2 was tested in the forward orientation to confirm the meter factor and demonstrate the reproducibility of the USM, which was found to be -0.025 %. Table 16 also presents the shift in the discharge coefficient between the CFD results and those from the ISO 5167-2 standard [3] for the forward orientation, as detailed in sections 3.1.5 and 3.2.5.

Table 16 – Results Summary

OP	Orientation	Flow Test OP Average Flow, Sm^3/h	Flow Test USM Average Flow, Sm^3/h	Shift in Discharge Coefficient, %			
				Flow Test: USM vs OP	NEL CFD Fluent	SUSU CFD Fluent	SUSU CFD CFX
No 1	Forward	153,153	157,583	MF = 0.9719	-0.54	-0.37	-0.38
	Reverse	**158,548**	**168,355**	**5.814**	**6.88**	**4.92**	**5.58**
No 2	Forward	157,612	157,651	-0.025	-0.53	-0.36	-0.37
	Reverse	**158,178**	**165,326**	**4.324**	**5.34**	**3.62**	**4.07**

The flow test results align closely with the CFD results supplied by both independent ITEs, as shown in Figure 20. This alignment enhances confidence in the obtained results, demonstrating the agreement between the theoretical modelling approach and the empirical flow test.

Flow testing, while providing valuable empirical data, is subject to several sources of uncertainty. In this study, the uncertainty of the flow tests was not assessed. However, the uncertainty of the USM is expected to be within 2 %, with an additional uncertainty of 0.3 % due to averaging and data logging frequency. Furthermore, the thickness of the pipe walls may introduce additional uncertainty due to the mismatch in acoustic impedance and potentially significant refraction.

Since the USM was corrected using the meter factor derived from the comparison with the orifice plate flow meter and was demonstrated to be reproducible between plates, a nominal 1 % error bar was applied in Figure 20 as a visual aid to illustrate the similarity between the methods, although it is not indicative of the actual uncertainties.

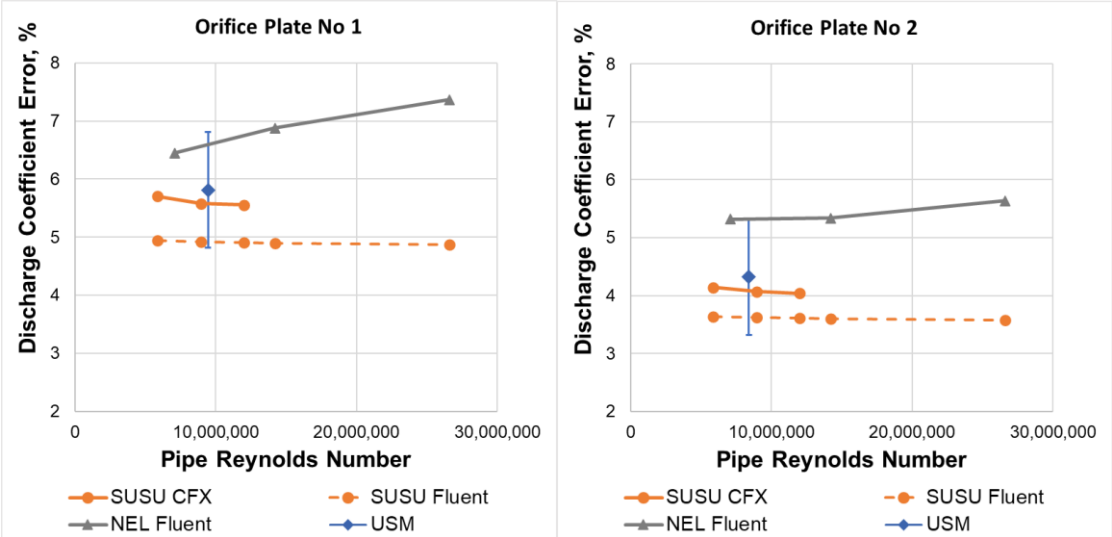

Figure 20 – Summary of Measurement Error Prediction Results

For both orifice plates, the CFX solver provided the CFD simulation results the closest to the flow test results. Based on the flow tests, orifice plate No 1 undermeasured by 5.814 % in the reverse orientation. This is compared to a 5.58 % undermeasurement predicted by the CFX solver, with a discrepancy of only 0.23 %. Similarly, flow testing showed that orifice plate No 2 undermeasured by 4.324 % in the reverse orientation, while the CFX solver predicted a 4.07 % undermeasurement, resulting in a difference of just 0.254 %.

5 CONCLUSION

Reversing an orifice plate can result in a significant measurement error. The magnitude of the error depends on the orifice plate beta ratio ‘β’, bore thickness ‘e’, plate thickness ‘E’, and Reynolds number, all of which vary, and there is currently no single best approach to assess and correct this error. A rough estimation can be made using published data [2] and [4], but if more accurate estimates are required, CFD analysis or flow tests, as detailed in this paper, should be considered.

The NEL assessment was completed using a single CFD solver, with the results described in section 3.1. The Emerson (SUSU) assessment was conducted with two different CFD solvers, and the results are described in section 3.2. The CFD models were validated by comparison with the ISO 5167-2 standard in the forward orientation and through a correlation based on previous calibration and test data of orifice plates installed in both forward and reverse orientations. Despite the results agreeing very well, there are still differences in the selected CFD models (mesh quality, turbulence model, boundary conditions, etc.) and solvers, there are small differences in plate geometries, small differences in process parameters, and finally the overall uncertainty in any modelling technique all provide

reasonable explanations for the differences observed. It can be observed that the CFD results from NEL and SUSU for the two cases presented in this paper (the Judy orifice plate results shown in Figure 11, and the results for the NTS offtake to LDZ orifice plates shown in Figure 20) follow a consistent pattern: the NEL results are higher than the experimental data, while SUSU results are lower, within comparable limits of 3 % and 1 %.

The i-Vigilant assessment was completed with a physical flow test using a clamp-on ultrasonic flowmeter at a single flowrate for both orifice plates, as detailed in section 4. The flow test was highly successful, with the results matching multiple CFD simulations within 2 %. This is particularly noteworthy given that the actual setup of the USM took around 30 minutes, requiring only the measurement of wall thickness and pipe circumference using a steel tape. It should be emphasised that the CFD results were found in good agreement with each other, as well as with the flow test results, which fell almost halfway between the two CFD simulations. This consistency provided confidence in the accuracy of the results, enabling the CFD to support a calculation for correcting the mismeasurement. Furthermore, based on CFD analysis, the correction was found to be practically independent of the Reynolds number, which eliminated the need for significantly more demanding and time-consuming flow tests.'

In summary, the decision was made to use the average of the predicted errors obtained from the NEL Fluent model and the SUSU CFX model. From Figure 20, this is the average of the circle and the triangle at the same Reynolds number as the diamond, which represents the flow test results. The variation in error over the Reynolds number range is relatively small, so to avoid a lengthy recalculation process, the decision was made to apply a constant correction factor for the measurement error correction. This factor was determined by interpolating between the modelled points at the Reynolds number the USM flow test was conducted. The final correction factor for orifice plate No 1 was found to be 1.06084, and for orifice plate No 2, 1.04709. The plates have the same beta ratio but differ in orifice bore thickness, plate thickness, and bevel angle. These differences in geometry of the orifice plates appear insignificant, but in reverse orientation, they resulted in a 1.3% difference in measurement error. This confirms the sensitivity of the measurement error to the orifice plate geometry, proving that each individual plate should be studied separately.

Overall, CFD provides detailed flow insights like velocity fields and pressure distributions, which are impossible with physical testing. It offers flexibility by simulating various conditions without extensive infrastructure and is cost-effective, as the model can be reused for different scenarios. However, CFD requires a complex setup, including precise geometry and boundary conditions, and faces uncertainty in turbulence modelling, particularly in complex flows. Additionally, validation against experimental data is essential to ensure accuracy.

In contrast, flow testing offers direct real-world data under actual operating conditions and requires no complex modelling. It can also be used for validating theoretical models like CFD, ensuring confidence in predictions. However, flow testing has uncertainties due to measurement and environmental factors, often comparable with CFD. It faces practical constraints, requiring physical access, precise meter alignment, and stable conditions, which may not always be possible. Additionally, it is generally more time-consuming than CFD, particularly for testing multiple scenarios.

While CFD offers flexibility, cost-effectiveness, and detailed flow insights, it requires careful setup and validation. On the other hand, flow testing provides direct real-world data but comes with practical limitations, such as available flowing regimes, capability of the instrumentation in use, logistics, and costs. A hybrid approach, combining CFD's detailed simulations with the validation of flow testing, could leverage the strengths of both methods for more accurate and reliable results.

6 ABBREVIATIONS

2D	two-dimensional
3D	three-dimensional
AGA	American Gas Association
ANSYS	High-performance computational fluid dynamics software tool
CAD	Computer Aided Design
CFD	Computational Fluid Dynamics
CFX, Fluent	ANSYS Solvers
CSV	Comma Separated Value
GC	Gas Chromatograph
GRI	Gas Research Institute
ISO	International Organization for Standardisation
ITE	Independent Technical Expert
LDZ	Local Distribution Zone
MF	Meter Factor
NEL	National Engineering Laboratory
NSFMW	North Sea Flow Measurement Workshop
NTS	National Transmission System
OP	Orifice Plate
RANS	Reynolds-Averaged Navier-Stokes equations
SMER	Significant Measurement Error Report
SST	Shear Stress Transport
SUSU	South Ural State University
UK	United Kingdom
USM	Ultrasonic Flow Meter
vs	versus

7 REFERENCES

[1] Brown, G.J., Reader-Harris, M.J., Gibson, J.J., National Engineering Laboratory UK; and G.J. Stobie, Phillips Petroleum Co UK Ltd. Correction of readings from an orifice plate installed in reverse orientation // 18th North Sea Flow Measurement Workshop, 2000.

[2] George, D.L, and Morrow, T. B, Orifice meter operational effects: Orifice meter calibration for backwards-facing orifice plates, GRI Report Number 01/0074

[3] ISO 5167-2:2003, Measurement of fluid flow by means of pressure differential devices inserted in circular cross-section conduits running full – Part 2: Orifice plates. A revised edition was published in 2022 and is currently available.

[4] Lawrence, P.A., The Effects of Orifice Plate Meters When Installed Backwards, A Technical Review, PAL Technical Services LLC, 2023.

[5] Menter, F.R., Two-equation eddy viscosity turbulence models for engineering applications. AIAA J. 32, No 1, pp.1299–1310, 1994.

[6] Schlichting H. Boundary Layer Theory, McGraw-Hill, New York, 1968.

[7] SHIH, T-H., LIOU, W. W., SHABBIR, A., and ZHU, J. A New k-e Eddy-Viscosity Model for High Reynolds Number Turbulent Flows - Model Development and Validation. Computers Fluids, 24(3): 227-238, 1995.

NOTATION

The symbols defined within the paper are listed below.

b	mm	difference orifice bore thickness and plate thickness
C	-	discharge coefficient
d	m	orifice bore diameter
D	m	internal pipe diameter
E	mm	orifice bore thickness
E	mm	plate thickness
Pup	Pa	upstream pressure
Px	Pa	pressure on a wall
Re_D	-	pipe Reynolds number
q_m	kg/s	mass flow rate
α	°	angle of bevel
β	-	diameter ratio
Δp	Pa	differential pressure
ε	-	expansibility factor
ρ_1	kg/m^3	upstream process density